effects of random SPE must be accounted for simultaneously because the integrated effect of GCR over the mission duration adds an unavoidable offset to the mission radiation exposure that must be considered in tandem with the solar activity cycle and proximity to the sun for the potential of SPE exposure.

Both of the flyby missions considered here pass inside a radius of 1 AU at some point. The EME mission actually passes inside the orbital radius of Venus and has a higher SPE radiation risk (a SPE scale factor of 2.6 for EME vs 1.9 for EVE). Consequently, the EME trajectory has a greater potential than the EVE 2010 scenario for a violation of the mission exposure guidelines. Such a risk would require additional mass for emergency shielding that may prove prohibitive. If the solar activity prediction in Fig. 2 is considering, the 2010 EVE mission would encounter Venus at the very beginning of the maximum activity buildup for solar period 24 and the 2006 EME mission would encounter Mars during an interval of decreased activity. The risk of increased likelihood of an SPE must be weighed in terms of the TransHab distance from the sun and the corresponding scaled exposure magnitude when comparing these two missions. Therefore, the increased risk of SPE occurrence in the EVE mission due to its timing with the beginning of greater solar activity is offset by the small violation (7 REM for the mission limit) of the exposure guidelines that would occur if the large 1972 SPE impacted with the trajectory near EVE mission day 115. One factor that cannot be assessed is the directionality of the SPE, which may or may not intersect a TransHab vehicle following either the EVE or EME trajectory.

Conclusions

An approximate radiation model for the continuous effects of GCR and the finite duration effects of random SPE occurrences has been presented. Ambient solar radiation is not considered because its effect is generally less than that of the GCR, which actually decreases with a small linear slope as a trajectory approaches the sun. A radiation exposure analysis for the EVE 2010 and EME 2006 trajectories was conducted to estimate the relative risks involved with each mission. The radiation model assumed a uniform 20-cm thickness water shield and included the effects of a SPE on the order of magnitude of the large 1972 SPE should such an event occur at different times throughout each mission. The EME trajectory passes closer to the sun during a period of lower solar activity, indicating a greater hazard if a less likely SPE were to occur. The EVE trajectory passes only within a Venus orbital radius of the sun during a time of increased solar activity, indicating less of a hazard should a more likely SPE occur. Given the relative radiation hazards presented here, the EVE 2010 mission is superior to the EME 2006 mission in terms of radiation exposure due to mission duration and proximity to the sun.

Acknowledgments

This work was supported in part by a Graduate Research Fellowship Grant from the National Science Foundation. Special thanks to Bedford Cockrell at NASA Johnson Space Center for suggesting the TransHab problem to us and for his helpful discussions.

References

[1]Crain, T., Bishop, R. H., Fowler, W., and Rock, K., "Interplanetary Flyby Mission Optimization Using a Hybrid Global–Local Search Method," *Journal of Spacecraft and Rockets*, Vol. 37, No. 4, 2000, pp. 468–474.

[2]Cocks, F. H., and Watkins, S., "Radiation Shielding for Interplanetary Spacecraft," Dept. of Mechanical Engineering and Materials Science, Duke Univ., Durham, NC, 1993.

[3]Letaw, J. R., and Clearwater, S., "Radiation Shielding on Long-Duration Space Missions," Severn Communications Corp., SCC Rept. 86-02, Severna Park, MD, July 1986.

[4]Conway, J. C., and Lawrence, W. T., "Radiation Shielding in Transit to Mars and on the Surface," *Mars: Past Present and Future*, 1st ed., AIAA, Washington, DC, 1992, pp. 239–253.

[5]Tribble, A. C., *The Space Environment: Implications for Spacecraft Design*, 1st ed., Princeton Univ. Press, Princeton, NJ, 1995, pp. 11–20, 137–162.

C. A. Kluever
Associate Editor

Payload Deployment by Reusable Launch Vehicle Using Tether

K. D. Kumar*
National Aerospace Laboratory, Tokyo 181 0015, Japan

Introduction

THE advent of communication satellites in polar orbits of 600–1200-km altitude and the development of the international space station (ISS) at 400-km altitude and 51.6-deg inclination have created an urgent need for low-cost access to such lower Earth orbits. The space tether can be a viable alternative to provide an answer to this need. The momentum transfer is one of the several important tether applications earlier proposed and analyzed.[1] Colombo et al.,[2] Bekey,[3] and Bekey and Penzo[4] have shown that tethered systems provide significant impulse saving for transfer missions from circular orbits. Kyroudis and Conway[5] have stated the advantage of an elliptically orbiting tethered dumbbell system for satellite transfer to geosynchronous altitude. The effects of various tether deployment schemes as well as the out-of-plane libration on payload orbit raising are studied by Kumar et al.[6]

Recently, Bekey[7] has shown the advantage of payload deployment by reusable launch vehicle (RLV) with tether compared to the RLV with upper stages. However, the system equations of motion have not been considered in his study and therefore the system parameters obtained by Bekey so as to deploy the payload at specified low-Earth circular orbit may differ from the results of the actual simulation study. The present investigation is undertaken with a view to circumvent these limitations as well as to carry out the detailed analysis.

Equations of Motion

The governing nonlinear, coupled ordinary differential equations of motion[8] of the system (Fig. 1) obtained by applying the Lagrangian formulation approach are as follows:

$$\ddot{R} = \dot{\theta}^2 R - \frac{\mu}{R^2} + \frac{3}{2}\frac{\mu}{R^2}\frac{M_e}{M}\frac{L}{R^2}(1 - 3\cos^2\beta\cos^2\eta)$$

$$\ddot{\theta} = -2\frac{\dot{R}}{R}\dot{\theta} - \frac{3}{2}\frac{\mu}{R^3}\frac{M_e}{M}\frac{L}{R^2}\sin 2\beta\cos^2\eta$$

$$\ddot{\beta} = 2\frac{\dot{R}}{R}\dot{\theta} - (\dot{\theta}+\dot{\beta})\left[(2+\mu_c)\frac{\dot{L}}{L} - 2\dot{\eta}\tan\eta\right] - \frac{3}{2}\frac{\mu}{R^3}\left(\sin 2\beta - \frac{M_e}{M}\frac{L}{R^2}\sin 2\beta\cos^2\eta\right)$$

$$\ddot{\eta} = -(2+\mu_c)\frac{\dot{L}}{L}\dot{\eta} - \frac{1}{2}(\dot{\theta}+\dot{\beta})^2\sin 2\eta - \frac{3}{2}\frac{\mu}{R^3}\cos^2\beta\sin 2\eta$$

$$\ddot{L} = \left[(\dot{\theta}+\dot{\beta})^2\cos^2\eta + \dot{\eta}^2 - \frac{\mu}{R^3}(1 - 3\cos^2\beta\cos^2\eta)\right]L - \mu_c\frac{L}{2}\left[3\frac{\dot{L}^2}{L^2} + (\dot{\theta}+\dot{\beta})^2\cos^2\eta + \dot{\eta}^2 - \frac{\mu}{R^3}(1 - 3\cos^2\beta\cos^2\eta)\right] - \frac{\mathrm{EA}}{M_e}\varepsilon_t U(\varepsilon_t) - 2\zeta\frac{\mathrm{EA}}{M_e L_0}(\dot{L} - \dot{L}_0) \quad (1)$$

where $\mu_c = (L/M_e)(\mathrm{d}M_e/\mathrm{d}L) = (1/M_e)(m_t/3)[(m_2 + m_t/2) - 2(m_1 + m_t/2)]$; ε_t = tether strain, $L/L_0 - 1$; $U(\varepsilon_t) = 1$ if $\varepsilon_t \geq 0$, 0

Received 28 October 1999; revision received 19 September 2000; accepted for publication 12 October 2000.

*Science and Technology Agency Fellow, Guidance and Control Laboratory, Flight Division, Osawa 6-13-1. Member AIAA.

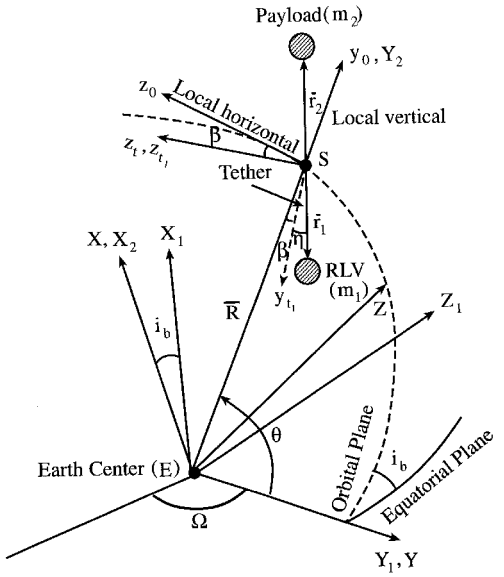

Fig. 1 Geometry of the system model.

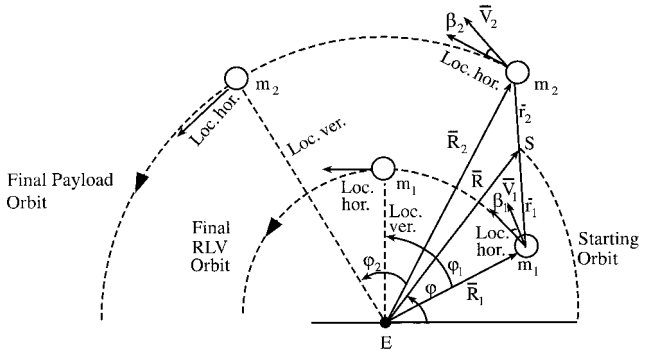

Fig. 2 Position and velocity of the RLV/payload at the release point.

if $\varepsilon_t < 0$; m_1, m_2, m_t = RLV, payload and tether ($\rho_t L_t$) masses, respectively; EA = tether modulus of rigidity; L = distance between two platform mass centers; L_0 = unstreched tether length; $M = m_1 + m_2 + m_t$ = total mass, and $M_e = (1/M)(m_1 + m_t/2)(m_2 + m_t/2) - m_t/6$ = equivalent system mass; R = orbital radius of the center of mass S of the system; β, η = tether in-plane and out-of-plane swing angle, respectively; θ = latitude argument of the center of mass S of the system; ζ = tether damping coefficient; μ = Earth's gravitational constant.

Release Conditions of RLV/Payload

Position and Velocity of RLV/Payload

The position and velocity of RLV and the payload at the instant of release (Fig. 2) are expressed as

$$R_i = -r_i \sin\eta \hat{I} + [R\cos\theta + r_i \cos\eta\cos(\theta+\beta)]\hat{J} + [R\sin\theta + r_i\cos\eta\sin(\theta+\beta)]\hat{K}, \qquad i = 1,2$$

$$V_i = -r_i\dot{\eta}\cos\eta\hat{I} + [\dot{R}\cos\theta - R\dot{\theta}\cos\theta - r_i\dot{\eta}\sin\eta\cos(\theta+\beta) - r_i(\dot{\theta}+\dot{\beta})\cos\eta\sin(\theta+\beta)]\hat{J} + [\dot{R}\sin\theta + R\dot{\theta}\cos\theta - r_i\dot{\eta}\sin\eta\sin(\theta+\beta) + r_i(\dot{\theta}+\dot{\beta})\cos\eta\cos(\theta+\beta)]\hat{K} \qquad i = 1,2 \quad (2)$$

where $\hat{I}$, $\hat{J}$, $\hat{K}$ are the unit vectors along S-XYZ frame. The corresponding magnitudes are given as

$$R_i = \left(R^2 + r_i^2 + 2Rr_i\cos\beta\cos\eta\right)^{\frac{1}{2}}, \qquad i = 1,2$$

$$V_i = \left\{\dot{R}^2 + R^2\dot{\theta}^2 + r_i^2\dot{\eta}^2 + r_i^2(\dot{\theta}+\dot{\beta})^2\cos^2\eta - 2\dot{R}r_i[\dot{\eta}\cos\beta\sin\eta + (\dot{\theta}+\dot{\beta})\sin\beta\cos\eta] + 2Rr_i\dot{\theta}[-\dot{\eta}\sin\beta\sin\eta + (\dot{\theta}+\dot{\beta})\cos\beta\cos\eta]\right\}^{\frac{1}{2}} \qquad i = 1,2 \quad (3)$$

where $r_1 = -[(m_2 + m_t/2)/M]L$; $r_2 = [(m_1 + m_t/2)/M]L$. Here, it is assumed that reel-in/reel-out operations have ended prior to the tether being cut ($\dot{r}_i = 0$).

Orbital Elements of RLV/Payload

The semimajor axes a_i and eccentricities e_i of the orbits of RLV ($i = 1$) and the payload ($i = 2$) after release can be written as[9]

$$a_i = \frac{R_i}{\left(2 - R_i V_i^2/\mu\right)}, \qquad e_i = \left[\left(\frac{R_i V_i^2}{\mu} - 1\right)^2 \cos^2\beta_i + \sin^2\beta_i\right]^{\frac{1}{2}} \qquad i = 1,2 \quad (4)$$

where β_i is the angle between the velocity $\boldsymbol{V}_i$ of mass m_i and the local horizontal (Fig. 2). The inclination of the plane of the released RLV/payload orbit to the starting orbital Y-Z plane i_{bi} is given in Ref. 9.

Release of RLV/Payload During Tether Mission

The release of RLV/payload should take place when maximum decrease of RLV altitude as well as the maximum gain of payload altitude occur. To satisfy these conditions, $\boldsymbol{R}_i$ and $\boldsymbol{V}_i$ must be perpendicular, i.e, $\beta_i = \pi/2$.

$$\boldsymbol{R}_i \cdot \boldsymbol{V}_i = 0, \qquad i = 1,2 \quad (5)$$

$$\dot{R}\left[\frac{1 + (r_i/R)\cos\beta\cos\eta}{r_i}\right] - \dot{\beta}\sin\beta\cos\eta + \dot{\eta}\cos\beta\sin\eta = 0 \quad (6)$$

Considering $r_1 \neq r_2$, we get the following conditions:

$$\dot{R} = 0, \qquad \dot{\beta}\tan\beta = \dot{\eta}\tan\eta \quad (7)$$

The solution to Eq. (7) is $\beta = \eta = 0$, i.e., the release of RLV/payload must take place when the tether is aligned with the local vertical during librations on forward swing. Substituting the preceding conditions in Eq. (2), the position and speed of RLV/payload at release point simplify to

$$R_i = R + r_i, \qquad i = 1,2 \quad (8)$$

$$V_i = \left[R^2\dot{\theta}^2 + r_i^2\dot{\eta}^2 + r_i^2(\dot{\theta}+\dot{\beta})^2 + 2Rr_i\dot{\theta}(\dot{\theta}+\dot{\beta})\right]^{\frac{1}{2}}, \qquad i = 1,2 \quad (9)$$

Applying Kepler's second law of planetary motion to obtain the expression for $\dot{\theta}$ (considering RLV/payload is released at an angle φ measured from the perigee, see Fig. 2), the preceding expression for speed of RLV/payload can be written as

$$V_i^2 = \frac{\omega_n^2 a^2}{(1-e^2)}\left((1+el)^2 + \hat{r}_i^2\lambda^2(1-e^2) + \frac{\hat{r}_i}{(1-e^2)^2}\left[(1+el)^2 + \delta(1-e^2)^{\frac{3}{2}}\right]\left\{\hat{r}_i\left[(1+el)^2 + \delta(1-e^2)^{\frac{3}{2}}\right] + 2(1+el)\right\}\right) \quad (10)$$

where $el = e\cos\varphi$; $\hat{r}_i = r_i/a$; $\dot{\theta} = h/R^2 = \omega_n(1+e\cos\varphi)^2(1-e^2)^{-3/2}$; h = system angular momentum per unit mass; $\varphi = \theta - \omega$; ω = argument of the perigee; δ = ratio of tether in-plane swing rate to the mean orbital rate, $\dot{\beta}/\omega_n$; λ = ratio of tether out-of-plane swing rate to the mean orbital rate, $\dot{\eta}/\omega_n$; ω_n = mean orbital rate, $(\mu/a^3)^{1/2}$.

Because $r_i \ll a$, this implies $\hat{r}_i \ll 1$, and Eq. (10) simplifies to

$$V_i^2 = \frac{\omega_n^2 a^2}{(1-e^2)}\left\{(1+e\cos\varphi)^2 + \frac{2\hat{r}_i(1+e\cos\varphi)}{(1-e^2)^2}\times\left[(1+e\cos\varphi)^2 + \delta(1-e^2)^{\frac{3}{2}}\right]\right\}, \qquad i = 1,2 \quad (11)$$

By substituting the preceding expression from Eq. (3), we can express the perigee height of RLV R_{h1} and apogee height of payload R_{h2} as

$$R_{hi} = a(1+e\cos\varphi) + r_i[7 + 4\delta + 4(5+\delta)e\cos\varphi], \qquad i = 1,2 \quad (12)$$

Table 1 RLV/payload altitude after its release using deployment schemes: a) EA, b) EAED

Payload mass m_2, kg	Tether length, km (a)/(b)	Eccentricity of starting RLV + payload orbit (a)/(b)	Predeployment true anomaly Ψ_0 (a)/(b), deg	Payload deployed at altitude, km	RLV placed at altitude, km	Maximum tether tension, N (a)/(b)
1000	15.3/18.6	0.0101/0.0099[a]	242.3/108.4	400	239	438/104
1000	52.9/68.5	0.0365/0.0352[a]	166.4/1.0	800	212	1395/428
1000	103.5/125.1	0.0599/0.0588[b]	43.1/34.5	1200	185	1198/772
2000	15.8/19.8	0.0102/0.0099[a]	238.1/98.2	400	229	652/201
2000	55.2/68.2	0.0363/0.0354[b]	158.5/119.7	800	175	1448/843
2000	105.9/149.3	0.0598/0.0575[c]	41.1/113.7	1200	125	1578/1593
4000	17.2/21.9	0.0102/0.0099[a]	228.2/79.1	400	208	750/414
4000	62.2/73.2	0.0356/0.0354[a]	145.1/53.4	800	101	2488/1825
4000	106.0/147.5	0.0606/0.0582[c]	38.9/187.2	1200	6	2312/3253

[a]Released at 4.5 orbits. [b]Released at 5.5 orbits. [c]Released at 6.5 orbits.

For minimum R_{h1} and maximum R_{h2}, we solve $\partial R_{hi}/\partial\theta = 0$, and we get the relation $\sin\varphi = 0$, $\varphi = k\pi$, $k = 0, 1, \ldots, n$. Thus, the minimum R_{h1} and the maximum R_{h2} occur at $\varphi = \pi, 3\pi, 5\pi, \ldots$ and $\varphi = 2\pi, 4\pi, 6\pi, \ldots$, respectively. That is to say, in case of elliptic starting orbit the maximum decrease of RLV altitude $(\Delta R_{h1})_{\max}$ occurs at apogee, and the maximum gain of payload altitude $(\Delta R_{h2})_{\max}$ occurs at perigee point, respectively, at zero libration angle on forward swing and are written as

$$(\Delta R_{hi})_{\max} = (-1)^i r_i\{7 + 4\,\delta[1 + (-1)^i e] + (-1)^i 20e\} \qquad i = 1, 2 \quad (13)$$

In case the starting orbit is circular (i.e., $e = 0$), the maximum decrease of RLV altitude as well as the maximum gain of payload altitude occur simultaneously when the libration angle is zero on forward swing and the preceding equation matches with the relation obtained by Kumar et al.[6]

Results and Discussion

With a view to assess the effectiveness of the proposed concept, the detailed system response is numerically simulated using Eq. (1). We assumed the following numerical data for the system: $m_1 = 14{,}000$ kg; $\rho_t = 1$ kg/km; $EA = 10^4$ N; $L_{\text{to}} = 10$ m; $\zeta = 0$; starting perigee of (RLV + payload) orbit = 6628 km; R_E = Earth radius = 6378 km. The system is assumed to enter the starting orbit with the initial conditions: $L = \beta = \dot{\beta} = \eta = \dot{\eta} = 0$.

The tether is deployed using swing (EA) release[6] as given next:

$$L_0 = L_{\text{to}} \exp[C(t - t_0)] \quad (14)$$

where L_{to} = initial tether length, $C = 0.0008$ for $L_0 < 100$ km, and $C = 0.0007$ for $L_0 \geq 100$ km are taken.

The RLV/payload is released on a forward swing when the libration angle is instantaneously zero. Here, we vary the predeployment true anomaly (Ψ_0) (i.e., the angle at which tether deployment starts) so that the forward swing zero libration is caused to occur nearly simultaneously with apogee passage for maximum decrease in altitude of RLV as starting orbit being elliptic. The objective here is to place the payload in a circular orbit.

Figure 3 shows the position of RLV/payload and length L along with in-plane swing angle β, respectively, for cases of 4000 kg of payload mass deployed at 400- and 800-km altitudes. It is found that the tether length requirement increases from 17.2 to 62.2 km for payload deployment from 400- to 800-km altitudes. The corresponding RLV altitude after its release decreases from 208 to 101 km. However, when the payload mass decreases from 4000 to 2000 kg, the RLV altitude after its release increases by 74 km, as expected (Fig. 3). To avoid drastic fluctuations of tether tension, the following exponential accelerated-exponential decelerated (EAED) deployment scheme[8] with modification $L_{t1} = L_{\max}/2$ is applied:

$$L_0 = L_{t0} \exp[C_1(t - t_0)] \quad \text{for} \quad L_{t0} \leq L_0 \leq L_{t1}$$

$$L_0 = L_{t1} + (C_1/C_2)(L_{\max} - L_{t1})\{1 - \exp[-C_2(t - t_1)]\} \quad \text{for} \quad L_{t1} < L_0 \quad (15)$$

where $C_1 = C_2 = C$, $L_{\max}$ = maximum tether length.

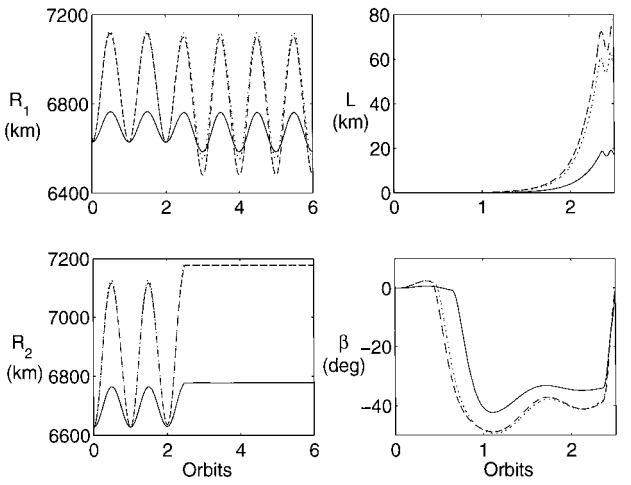

Fig. 3 Position of RLV/payload, length L, and in-plane swing angle β during tether release for cases: ——, payload mass of 4000 kg deployed at 400 km, tether deployment starts at 0.64 orbits and completed at 2.34 orbits; –·–, payload mass of 4000 kg deployed at 800 km, tether deployment starts at 0.40 orbits and completed at 2.32 orbits; and . . . . . , payload mass of 2000 kg deployed at 800 km, tether deployment starts at 0.44 orbits and completed at 2.33 orbits.

The results for different cases are summarized in Table 1. The RLV/payload is released at 2.5 orbits. It is observed that the application of EAED deployment scheme leads to the reduction of tether tension by 35–76% depending upon the payload mass and its final desired altitude except for longer tether lengths. When the payload mass is low and it is to be deployed at lower altitude signified by shorter tether length, there is a maximum decrease of tether tension compared to the EA deployment scheme, i.e., 76% for a case of payload mass of 1000 kg deployed at 400-km altitude. However, the EAED deployment scheme leads to increase in tether length requirements as well as the release of RLV/payload takes place just prior to 4.5 or 5.5 or 6.5 orbits instead of earlier release at 2.5 orbits. To accomplish the task of payload deployment based on the preceding results, the starting (RLV + payload) altitude and velocity should be $6628 \times (1 - e)^{-1}$ km and $2452.32 \times (1 + e)^{1/2}$ m/s, respectively. The maximum decrease in perigee height of RLV in Table 1 closely matches the results predicted by Eq. (13) within a maximum error of 500 m for EA deployment scheme and the error is within 2 km for EAED scheme.

Conclusions

We have investigated the payload deployment by reusable launch vehicle using a tether. The numerical performance results for a generic RLV are presented. These results, obtained by numerically integrating the governing nonlinear equations of motion of the tethered system, establish the feasibility of the concept. It is shown that the payload deployment to lower Earth circular orbits of 400–1200-km altitude along with the production of the reentry trajectory of RLV without using propulsive orbital maneuvering system is feasible. The concept proposed may be promising for future space missions involving RLV.

References

[1]Cosmo, M. L., and Lorenzini, E. L. (eds.), *Tethers in Space Handbook*, 3rd ed., Smithsonian Astrophysical Observatory, NAG8-1160, Cambridge, MA, Dec. 1997.

[2]Colombo, G., Martinez-Sanchez, M., and Arnold, D., "Use of Tethers for Payload Orbit Transfer," Smithsonian Astrophysical Observatory, NAS 8-33691, Cambridge, MA, March 1982.

[3]Bekey, I., "Tethers Open New Space Options," *Astronautics and Aeronautics*, Vol. 21, No. 4, 1983, pp. 33–40.

[4]Bekey, I., and Penzo, P. A., "Tether Propulsion," *Aerospace America*, Vol. 24, No. 7, 1986, pp. 40–43.

[5]Kyroudis, G. A., and Conway, B. A., "Advantages of Tether Release of Satellites from Elliptic Orbits," *Journal of Guidance, Control, and Dynamics*, Vol. 11, No. 5, 1988, pp. 441–448.

[6]Kumar, K., Kumar, R., and Misra, A. K., "Effects of Deployment Rates and Librations on Tethered Payload Raising," *Journal of Guidance, Control, and Dynamics*, Vol. 15, No. 5, 1992, pp. 1230–1235.

[7]Bekey, I., "Tethering a New Technique for Payload Deployment," *Aerospace America*, Vol. 35, No. 3, 1997, pp. 36–42.

[8]Zhu, R., Misra, A. K., and Lin, H., "Dynamics of Tether-Assisted Reentry Vehicle Systems," *AAS/GSFC International Symposium on Space Flight Dynamics*, Vol. 84, Advances in the Astronautical Sciences, 1993, pp. 1230–1235.

[9]Thompson, W. T., *Introduction to Space Dynamics*, Wiley, New York, 1961.

C. A. Kluever
Associate Editor

Thermal Protection System Materials and Costs for Future Reusable Launch Vehicles

D. J. Rasky,* F. S. Milos,† and T. H. Squire‡
NASA Ames Research Center,
Moffett Field, California 94035-1000

Nomenclature

$A(i, n)$	=	$i(1+i)^n/[(1+i)^n - 1]$, amortization function
C_{fab}	=	$C_{\text{purch}} + C_{\text{pers}} h_{\text{inst}}$, installed cost of material, \$/ft^2
$C_{\text{i/r}}$	=	$C_{\text{pers}}\, h_{\text{i/r}}$, cost for inspection and repair, \$/ft^2
C_{payl}	=	payload cost to orbit, \$/(lbm payload)
C_{pers}	=	personnel cost, including both direct and indirect costs, \$/hr
C_{purch}	=	purchase cost, \$/ft^2
F_{rate}	=	flight rate, #/yr
F_{sp}	=	$(N_{\text{limit}} - 1)\, f_{\text{damage}}$, TPS spares fraction (minimum)
f_{amort}	=	$N_{\text{limit}}\, A(f_i/F_{\text{rate}}, N_{\text{limit}})$, amortization factor
f_{damage}	=	damage replacement fraction, %/flt
f_i	=	yearly interest rate, %
f_{payl}	=	payload conversion factor, (lbm payload)/(lbm TPS)
h_{inst}	=	installation time, hr/ft^2
$h_{\text{i/r}}$	=	inspection and repair time, hr/ft^2
N_f	=	total number of flights, #
N_{life}	=	TPS reuse flight limit, #
N_{limit}	=	$\min(N_f, N_{\text{life}})$, #
T_{max}	=	maximum reuse temperature, °F
W_{area}	=	areal weight, (lbm TPS)/ft^2
\$	=	life-cycle cost parameter, \$/ft^2-flt

Received 11 May 2000; revision received 21 September 2000; accepted for publication 8 October 2000.

*Senior Scientist, Space Technology Division, MS 229-3. Senior Member AIAA.

†Ceramic Engineer, Thermal Protection Materials and Systems Branch, MS 234-1. Senior Member AIAA.

‡Senior Research Scientist, ELORET Corp., MS 234-1.

Introduction

THERE is considerable interest in developing new reusable launch vehicles (RLVs) for reducing the cost of transporting payload to and from orbit.[1–3] This work reviews 13 candidate thermal protection system (TPS) options currently available for RLVs. It is useful to begin with the current Space Shuttle TPS layout as a reference.[4] The nose cap and wing leading edge, which reach the highest temperatures, are made of reinforced carbon-carbon (RCC) that is protected from oxidation by an external coating (~0.020 in. thick) of silicon-carbide. Most of the windward surface consists of 9 lb/ft^3 ceramic tiles (LI-900) with a thin (~0.012 in.) coating of reaction cured glass (RCG). The leeward side of the vehicle is covered largely by advanced flexible reusable surface insulation (AFRSI), a quilted ceramic blanket, and FRSI, a polyamide felt. These four materials can be considered to be first generation reusable TPS. Since the time of the Space Shuttle design, considerable progress has been made advancing TPS technologies in terms of thermal performance, robustness, and cost. For each of the major systems a second generation ceramic TPS has been developed, tested, and characterized. Metallic-based systems have also been developed.[5,6]

For applications requiring RCC in the past, advanced carbon-carbon (ACC) is now available.[7] This material has better mechanical properties, somewhat higher temperature capability to 2900°F, and greatly increased oxidation resistance. New carbon fiber-reinforced silicon-carbide matrix composites (C/SiCs) have shown additional improvement in properties over ACC with use temperatures to 3000°F and above.[8] For rigid tiles NASA Ames Research Center has made two significant advancements. The first is a tile substrate called alumina enhanced thermal barrier (AETB),[9] which incorporates alumina fibers for improved dimensional stability at high temperatures, to 2600°F and above. This material can be made to densities as low as 8 lb/ft^3. The second is a coating preparation called toughened uni-piece fibrous insulation (TUFI),[10] which penetrates about 0.1 in. into the tile substrate. The resulting composite, with a density gradient near the surface, provides orders of magnitude increased damage resistance compared with RCG-coated LI-900, with only a small weight increase. The TPS that combines these two developments is called AETB-8/TUFI and has been adopted for high damage areas on the Space Shuttle Orbiters.

Two notable developments have occurred in flexible ceramic blanket technology. The first is aluminoborosilicate-based fibers with use temperatures of 2000°F and above,[11] in comparison to quartz and silica fiber used in AFRSI, which have multiuse temperature limits of 1200–1400°F. Blankets incorporating these new high-temperature fibers are referred to as AFRSI-HT.[12] The second is an integral weaving technique that produces a fluted core blanket with a smoother surface and greater resistance to aeroacoustic noise, to levels as high as 170 dB.[13] This NASA Ames Research Center innovation is called tailorable advanced blanket insulation (TABI). Finally, for felt-based TPS Boeing is developing polybenzimidazole blanket insulation (PBI), with a multiuse temperature limit of 1000°F and above, in contrast to shuttle FRSI, which has a multiuse temperature limit of about 700°F.

NASA Langley Research Center and BF Goodrich (formerly Rohr Corp.) have led the development of metallic-based TPS.[5,6] This activity uses essentially three approaches: metallic tiles, which encase a fibrous ceramic batting in a box fabricated largely from metallic honeycombs, typically nickel-based alloys; metallic honeycomb sheets, made of nickel-based alloys, incorporating a fibrous back-side insulation encapsulated in a metallic foil bag, providing reduced weight; and metallic multiwall, which is comprised of dimpled titanium metal sheets, which are stacked and then diffusion bonded at contact points to form the TPS. The nickel-based systems can be used up to temperatures of about 1800°F and the titanium system to about 1100°F.

These 13 TPS materials have various benefits and limits in terms of temperature capability, weight, initial cost, and maintenance. Carbon-carbon and C/SiC systems have the highest temperature capability but are relatively expensive and heavy, requiring significant